Thermal diffusivity measurements of thin plates and filaments using lock-in thermography

Arantza Mendioroz, Raquel Fuente-Dacal, Estibaliz Apiñaniz, and Agustín Salazar[a)]
Departamento de Física Aplicada I, Escuela Técnica Superior de Ingeniería, Universidad del País Vasco, Alameda Urquijo s/n, 48013 Bilbao, Spain

(Received 18 May 2009; accepted 21 June 2009; published online 23 July 2009)

Photothermal radiometry has been widely used to measure the thermal diffusivity of bulk materials. In the case of thin plates and filaments, a one-dimensional heat propagation model including heat losses has been developed, predicting that the thermal diffusivity can be obtained by recording both the surface temperature amplitude and phase profile slopes ("slope method"). However, this method has given highly overestimated values of the thermal diffusivity of poor-conducting films and filaments. In this paper we analyze the effect of the experimental factors affecting the thermal diffusivity measurements of thin plates and filaments using infrared thermography, in order to establish the experimental conditions needed to obtain accurate and reliable values of the diffusivity of any kind of material using the slope method. We present the calculations of the surface temperature of thin isotropic and anisotropic plates heated by a modulated and tightly focused laser beam, showing that the slope method is also valid for this kind of pointlike heating. Special attention is paid to the effect of surface heat losses (convective and radiative) on the diffusivity measurements of small-dimension and poor-conducting materials. Lock-in thermography measurements performed in the best experimental conditions on a wide set of samples of different thermal properties (thin isotropic and anisotropic plates and filaments) confirm the validity of the slope method to measure accurately the thermal diffusivity of samples of these shapes. © *2009 American Institute of Physics.* [DOI: 10.1063/1.3176467]

I. INTRODUCTION

Modulated photothermal radiometry (PTR) consists in illuminating the sample by an intensity modulated light beam and detecting the oscillating component of the temperature rise by means of an infrared detector connected to a lock-in amplifier. As the temperature rise depends on the thermo-optical properties of the sample, PTR has been widely used to measure the thermal diffusivity of a wide variety of materials. Moreover, the development of infrared video cameras with fast data acquisition (thousands of images/s) and high lateral resolution (tens of micrometer) provides powerful tools for the fast thermal characterization of large samples. The name of photothermal radiometry refers to the use of a single infrared detector, while lock-in thermography is used when the infrared emission is collected by a focal plane array of infrared detectors.

By tightly focusing the light beam onto the sample surface and by performing a radial scan of the PTR signal, the thermal diffusivity (D) can be retrieved. In the absence of heat losses, there is a linear relation between the phase of the surface temperature (ψ) and the lateral distance to the heating spot, with a slope $m=-\sqrt{\pi f/D}$, from which the thermal diffusivity can be obtained ("phase method").[1,2] However, the PTR signal is not only proportional to the surface temperature but it is also affected by the diffraction introduced by the detection optics and by the nonlinear effects produced by the sample heating. The result is an increase of the slope m (i.e., D is overestimated) for moderate heating powers, and even a loss of the linearity for strong heating powers.[3–7] The disturbing effects of diffraction and sample heating increase for low thermal diffusivity materials and high frequencies. A simple way to overcome this issue is to work at low modulation frequencies. However, in this case the presence of heat losses by radiation and convection modifies the temperature profile of the sample with respect to that obtained from a pure conductive model. This effect is especially strong when measuring the thermal diffusivity of thin plates or thin filaments since heat losses increase with the surface to volume ratio. That is the reason why heat losses are negligible for bulk samples (except at very low modulation frequencies) but become noticeable for thin plates and filaments.

In the case of one-dimensional (1D) heat propagation, i.e., the illumination covers the full width of a thin sample, it has been demonstrated that heat losses modify the slope of both the phase, ψ, and the natural logarithm of the amplitude of the oscillating temperature, $\ln(T)$, in such a way that the product of both slopes cancels the effect of heat losses: $m_\psi \times m_{\ln(T)}=-\pi f/D$.[8–10] This method works very well for good thermal conductors (metals, alloys, SiC, etc.),[2,8–11] but it fails when dealing with thin films and filaments of low thermal conductivity. For instance, the thermal diffusivities of a 76 μm thick plastic packing film and a 25 μm thick polyimide film were found to be 0.52 and 1.12 mm^2/s, respectively.[2,8] Both values are very much higher than the typical thermal diffusivity of polymers (0.1–0.2 mm^2/s).

[a)]Electronic mail: agustin.salazar@ehu.es.

 © 2009 American Institute of Physics

Author complimentary copy. Redistribution subject to AIP license or copyright, see http://rsi.aip.org/rsi/copyright.jsp

On the other hand, thermal diffusivity values of human hair in the range of 2–4 mm^2/s, an anomalously high value for a biological sample, have been reported.[12]

The aim of this work is to identify the influence of the experimental conditions on the thermal diffusivity measurements using the slope method, in order to extend its applicability to materials of any kind of thermal properties and shapes. We focus on thin plates and filaments, because of the great interest of characterizing the thermal properties of very thin objects, and because the effect of heat losses is meant to strongly affect the surface thermal field. We are especially interested in understanding and overcoming the overestimations of the thermal diffusivity of poor thermal conductors that have been found in literature. In this paper, we present the calculation of the temperature of isotropic and anisotropic thin plates [two dimensional (2D) heat propagation)], including the effect of heat losses, when they are illuminated by a focused and modulated light beam. It will be shown that, as already demonstrated in 1D propagation, the effect of radiation can be overcome by using both the amplitude and the phase of the PTR signal in the case of 2D heat propagation (pointlike illumination of a thin sample), but not in the case of three-dimensional heat propagation (pointlike illumination of a thick sample). Moreover, it will be demonstrated that the effect of convection is extremely high for this kind of sample shapes, but it can be overcome by enclosing the sample in a vacuum chamber. The effects of other experimental factors and limitations (such as diffraction, finite sample dimensions, and black layer used to improve the infrared emissivity) on the thermal diffusivity obtained from the slope method will be discussed in detail, for all kind of materials and modulation frequencies. Systematic lock-in thermography measurements performed with the optimum experimental conditions on thin plates and thin filaments of both good (metals and alloys) and poor (polymers and human hair) thermal conductors, as well as anisotropic materials, confirm the theoretical model and the ability of this technique to provide accurate thermal diffusivity measurements, provided that the restrictions imposed by the model are experimentally fulfilled.

II. THEORY

In this section, the oscillating temperature of an opaque sample illuminated by a modulated and tightly focused laser beam is calculated. Three geometries are studied: an isotropic slab, an anisotropic slab and a thin wire.

A. Isotropic slab

Let us consider a slab of thickness ℓ, illuminated by a laser beam of power P_o with a Gaussian profile of radius a (at $1/e^2$) and modulated at a frequency f ($\omega=2\pi f$). The geometry of the problem is shown in Fig. 1. Due to the cylindrical symmetry the problem, the oscillating component of the temperature can be written in the Hankel space as[13]

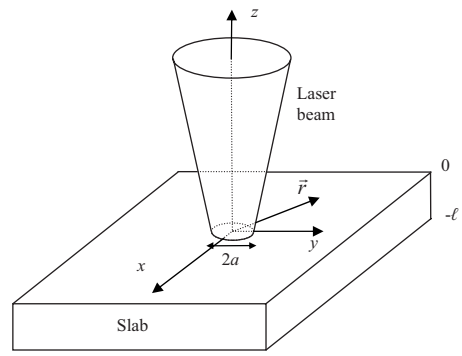

FIG. 1. Diagram of a slab illuminated by a focused light beam.

$$T_{ac}(r,z) = \int_0^\infty \delta J_0(\delta r)[Ae^{\beta z} + Be^{-\beta z}]d\delta, \tag{1}$$

where δ is the Hankel variable, J_0 is the Bessel function of the zeroth order and $\beta^2=\delta^2+\sigma^2$, being $\sigma=\sqrt{i\omega/D}$ the thermal wave vector. A and B are constants to be determined according to the boundary conditions, heat flux continuity, at the sample surfaces:

$$K \left.\frac{\partial T_{ac}}{\partial z}\right|_{z=0} + h_0 T_{ac}|_{z=0} = \frac{P_o}{4\pi}\int_0^\infty \delta J_0(\delta r)e^{-(\delta a)^2/8}d\delta, \tag{2a}$$

$$K \left.\frac{\partial T_{ac}}{\partial z}\right|_{z=-\ell} - h_1 T_{ac}|_{z=-\ell} = 0, \tag{2b}$$

where K is the thermal conductivity of the sample and h_0 and h_1 are the heat transfer coefficients at the upper and lower surfaces, respectively, which account for heat losses. It is assumed that the temperature rise is small, in such a way that the rate of heat dissipated from the slab surfaces can be regarded as a linear function of the temperature. The second term in Eq. (2a) is the Hankel transform of the heating power distribution of a Gaussian laser beam $(P_o/\pi a^2)e^{-2r^2/a^2}$. By substituting Eq. (1) into Eq. (2) the constants A and B are determined and the sample temperature is obtained

$$T_{ac}(r,z) = \frac{P_o}{4\pi K}\int_0^\infty \delta J_o(\delta r)\frac{e^{-(\delta a)^2/8}}{\beta} \times\left[\frac{(1+H_1)e^{\beta\ell}e^{\beta z} + (1-H_1)e^{-\beta\ell}e^{-\beta z}}{(1+H_0)(1+H_1)e^{\beta\ell} - (1-H_0)(1-H_1)e^{-\beta\ell}}\right]d\delta, \tag{3}$$

where $H_0=h_0/K\beta$ and $H_1=h_1/K\beta$. In this calculation, the heat conduction to the gas surrounding the slab is neglected due to its low thermal conductivity.

Two extreme cases of practical interest are as follows:

(a) The slab is thermally thin (i.e., $\ell \ll \mu=\sqrt{D/\pi f}$, the thermal diffusion length). Accordingly, $e^{\pm\beta\ell}\approx 1\pm\beta\ell$ and $h_0\approx h_1\approx h$. Now Eq. (3) reduces to

$$T_{ac}(r) = \frac{P_o}{4\pi K\ell}\int_0^\infty \delta J_o(\delta r)\frac{e^{-(\delta a)^2/8}}{\beta'^2}d\delta, \tag{4}$$

where $\beta'^2=\delta^2+\sigma'^2$, with $\sigma'^2=\sigma^2+(2h/K\ell)$. Note that the oscillating temperature does not depend on z. It is worth noting that for a given value of the heat transfer

Author complimentary copy. Redistribution subject to AIP license or copyright, see http://rsi.aip.org/rsi/copyright.jsp

coefficient h, the effect on the sample temperature increases for thin samples of low thermal conductivity. In particular, for a tightly focused laser beam ($a=0$) Eq. (4) reduces to

$$T_{ac}(r,a=0)=\frac{P_o}{4\pi K\ell}K_o(\sigma' r), \tag{5}$$

where K_0 is the zeroth order of the Kelvin function, and represents a cylindrical thermal wave propagating through the radial direction. Using the asymptotic approach for large r values[14] Eq. (5) reduces to

$$T_{ac}(r\to\infty,a=0)\approx\frac{P_o}{4\pi K\ell}\sqrt{\frac{\pi}{2\sigma'}}\frac{e^{-\sigma' r}}{\sqrt{r}}$$
$$=\frac{P_o}{4\pi K\ell}\sqrt{\frac{\pi}{2}}\frac{1}{\sqrt{\sigma_R'+i\sigma_I'}}\frac{e^{-\sigma_R' r}}{\sqrt{r}}e^{-i\sigma_I' r}, \tag{6}$$

where σ_R' and σ_I' are the real and the imaginary parts of σ'. As can be seen in Eq. (6), the phase of the temperature has a linear dependence on r whose slope is $m_\psi=-\sigma_I'$. On the other hand, the natural logarithm of the temperature amplitude multiplied by $\sqrt{r}$ also has a linear dependence on r whose slope is $m_{\ln(\sqrt{r}T)}=-\sigma_R'$. As can be seen both slopes are affected by heat losses, in fact $m_{\ln(\sqrt{r}T)}>m_\psi$. Accordingly, if one tries to obtain the thermal diffusivity from the slope of only the amplitude (phase), the value obtained will be overestimated (underestimated). However, their product $m_{\ln(\sqrt{r}T)}\times m_\psi=-\pi f/D$ is independent of heat losses and allows to obtain the thermal diffusivity of the thin slab. Finite laser spot sizes ($a\neq 0$) only affect the shape of the temperature amplitude and phase close to the laser spot, while at large r distances both slopes remain unchanged.

(b) The material is thermally thick (i.e., $\ell\gg\mu=\sqrt{D/\pi f}$). In this case $e^{-\beta\ell}\approx 0$, and according to Eq. (3) the surface temperature is given by

$$T_{ac}(r,z=0)=\frac{P_o}{4\pi K}\int_0^\infty \delta J_o(\delta r)\frac{e^{-(\delta a)^2/8}}{\beta+\frac{h_o}{K}}d\delta. \tag{7}$$

Equation (7) has no analytical solution, even in the case of negligible laser beam radius ($a=0$). However, from numerical simulations several conclusions are obtained. In the absence of heat losses, the natural logarithm of the temperature amplitude multiplied by r and the phase have a linear dependence on r with the same slope $m=-\sqrt{\pi f/D}$. The effect of heat losses is to change both slopes in the same manner as happens with thin slabs. However, this change in slope is not the same for the amplitude as for the phase and therefore their product does not give the thermal diffusivity of the sample ($m_{\ln(rT)}\times m_\psi\neq-\pi f/D$). Anyway, it is worth mentioning that the effect of heat losses in thick samples is small even for samples of low thermal conductivity. Only at very low frequencies ($f<0.1$ Hz) these losses should be taken into account.

B. Anisotropic slab

Now we consider the same slab as in Sec. II A, but with a thermal conductivity varying with the direction. Let the axes (x,y,z) in Fig. 1 be the principal axes of the anisotropic sample with the corresponding principal thermal conductivities (K_x,K_y,K_z) and thermal diffusivities (D_x,D_y,D_z). Due to the lack of cylindrical symmetry the ac component of the temperature can be expressed in the Fourier space as[15]

$$T_{ac}(x,y,z)=\int_{-\infty}^{\infty}\int_{-\infty}^{\infty}e^{-i(x\lambda+y\eta)}[A'e^{\gamma z}+B'e^{-\gamma z}]d\lambda d\eta, \tag{8}$$

where λ and η are the Fourier variables, and $\gamma^2=(D_x\lambda^2+D_y\eta^2+i\omega)/D_z$. A' and B' are constants to be determined from the heat flux continuity at the sample surfaces:

$$K_z\left.\frac{\partial T_{ac}}{\partial z}\right|_{z=0}+h_0T_{ac}|_{z=0}$$
$$=\frac{P_o}{4\pi}\int_{-\infty}^{\infty}\int_{-\infty}^{\infty}e^{-i(x\lambda+y\eta)}e^{-(\lambda^2+\eta^2)a^2/8}d\lambda d\eta, \tag{9a}$$

$$K_z\left.\frac{\partial T_{ac}}{\partial z}\right|_{z=-\ell}-h_1T_{ac}|_{z=-\ell}=0, \tag{9b}$$

where the second term in Eq. (9a) is the Fourier transform of the heating power distribution. By substituting Eq. (8) into Eqs. (9) the constants A' and B' are determined and the sample temperature is obtained

$$T_{ac}(x,y,z)=\frac{P_o}{4\pi K_z}\int_{-\infty}^{\infty}\int_{-\infty}^{\infty}e^{-i(x\lambda+y\eta)}\frac{e^{-(\lambda^2+\eta^2)a^2/8}}{\gamma}$$
$$\times\left[\frac{(1+H_1')e^{\gamma\ell}e^{\gamma z}+(1-H_1')e^{-\gamma\ell}e^{-\gamma z}}{(1+H_o')(1+H_1')e^{\gamma\ell}-(1-H_0')(1-H_1')e^{-\gamma\ell}}\right]d\lambda d\eta, \tag{10}$$

where $H_0'=h_0/K_z\gamma$ and $H_1'=h_1/K_z\gamma$. Now we analyze two extreme cases of practical interest:

(a) If the slab is thermally thin (i.e., $\ell\ll\mu_z=\sqrt{D_z/\pi f}$) Eq. (10) reduces to

$$T_{ac}(x,y)=\frac{P_o}{4\pi\rho c\ell}\int_{-\infty}^{\infty}\int_{-\infty}^{\infty}e^{-i(x\lambda+y\eta)}$$
$$\times\frac{e^{-(\lambda^2+\eta^2)a^2/8}}{D_x\lambda^2+D_y\eta^2+i\omega+\frac{2h}{\rho c\ell}}d\lambda d\eta, \tag{11}$$

where $\rho c=K_x/D_x=K_y/D_{y=}=K_z/D_z$ is the heat capacity. Note that the temperature does not depend on K_z or D_z. For a highly focused laser beam ($a=0$) Eq. (11) has analytical solution for the temperature along the principal axes

$$T_{ac}(x,a=0)=\frac{P_o}{2\rho c\ell}\frac{1}{\sqrt{D_xD_y}}K_o(\sigma_x' x), \tag{12a}$$

Author complimentary copy. Redistribution subject to AIP license or copyright, see http://rsi.aip.org/rsi/copyright.jsp

$$T_{ac}(y,a=0)=\frac{P_o}{2\rho c\ell}\frac{1}{\sqrt{D_xD_y}}K_o(\sigma'_y y), \tag{12b}$$

where $\sigma'^2_{x,y}=(i\omega/D_{x,y})+(2h/K_{x,y}\ell)$. Using the asymptotic approach for large x and y values,[14] Eq. (12) reduce to

$$T_{ac}(x\to\infty,a=0)\approx\frac{P_o}{2\rho c\ell}\frac{1}{\sqrt{D_xD_y}}\sqrt{\frac{\pi}{2\sigma'_x}}\frac{e^{-\sigma'_x x}}{\sqrt{x}}$$
$$=\frac{P_o}{2\rho c\ell}\frac{1}{\sqrt{D_xD_y}}\sqrt{\frac{\pi}{2}}\frac{1}{\sqrt{\sigma'_{xR}+i\sigma'_{xI}}}\frac{e^{-\sigma'_{xR}x}}{\sqrt{x}}e^{-i\sigma'_{xI}x}, \tag{13a}$$

$$T_{ac}(y\to\infty,a=0)\approx\frac{P_o}{2\rho c\ell}\frac{1}{\sqrt{D_xD_y}}\sqrt{\frac{\pi}{2\sigma'_y}}\frac{e^{-\sigma'_y y}}{\sqrt{y}}$$
$$=\frac{P_o}{2\rho c\ell}\frac{1}{\sqrt{D_xD_y}}\sqrt{\frac{\pi}{2}}\frac{1}{\sqrt{\sigma'_{yR}+i\sigma'_{yI}}}\frac{e^{-\sigma'_{yR}y}}{\sqrt{y}}e^{-i\sigma'_{yI}y}, \tag{13b}$$

where σ'_{xR}, σ'_{yR} and σ'_{xI}, σ'_{yI} are the real and the imaginary parts of σ'_x and σ'_y, respectively. As it happened with the isotropic thin slab, the phase and the natural logarithm of the temperature amplitude multiplied by $\sqrt{x}$ or $\sqrt{y}$ have a linear dependence on the distance in such a way that the product of the slopes is equal to $-\pi f/D_x$ or $-\pi f/D_y$, indicating that it is independent of heat losses. Accordingly, the thermal diffusivity along the principal axes can be obtained. Finite laser spot sizes ($a\neq 0$) do not affect the slopes.

(b) The material is thermally thick (i.e., $\ell \gg \mu_z=\sqrt{D_z/\pi f}$). In this case $e^{-\beta\ell}\approx 0$, and according to Eq. (3) the surface temperature is given by

$$T_{ac}(x,y,z=0)$$
$$=\frac{P_o}{4\pi K_z}\int_{-\infty}^{\infty}\int_{-\infty}^{\infty}e^{-i(x\lambda+y\eta)}\frac{e^{-(\lambda^2+\eta^2)a^2/8}}{\gamma+\frac{h_0}{K_z}}d\lambda d\eta. \tag{14}$$

Numerical simulations of Eq. (14) indicate that in the absence of heat losses, the natural logarithm of the temperature amplitude multiplied by x or y and the phase have a linear dependence on the distance with the same slope $-\sqrt{\pi f/D_x}$ or $-\sqrt{\pi f/D_y}$. For non-negligible heat losses, both slopes are modified in such a way that their product is not independent of heat losses. Anyway, as in the case of isotropic samples, the effect of heat losses on thick samples is almost negligible.

C. Thin filament

Now we recall the expression for the oscillating temperature of a thin filament of radius b, illuminated by a focused laser beam modulated at a frequency f (see Fig. 2). Outside the illuminated region, a perfectly 1D temperature oscillation is obtained whose value is given by[10]

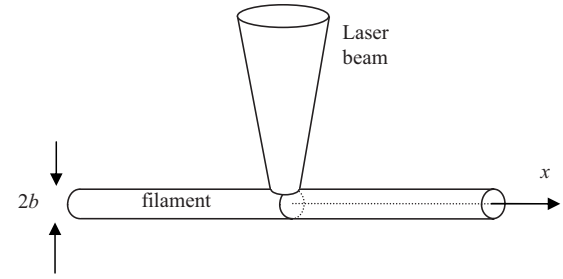

FIG. 2. Diagram of a filament illuminated by a focused light beam.

$$T(x)=\frac{T_o}{K\sigma''}e^{-\sigma'' x}=\frac{T_o}{K}\frac{1}{\sigma''_R+i\sigma''_I}e^{-\sigma''_R x}e^{-i\sigma''_I x}, \tag{15}$$

where T_o is a constant depending on the laser power and shape, and on the radius of the wire, $\sigma''^2=\sigma^2+(2h/Kb)$, and σ''_R and σ''_I are the real and the imaginary parts of σ''. It is worth noting that this solution is valid not only for opaque wires but for transparent ones as well. As for thin slabs, the slopes of both the natural logarithm of the amplitude and the phase of the temperature are affected by heat losses, being $m_\psi < m_{\ln(T)}$, while its product $m_\psi \times m_{\ln(T)}=-\pi f/D$ is independent of them, and therefore the thermal diffusivity of the fiber can be obtained in a easy manner. As also occurs in the case of slabs, if heat losses are negligible ($h=0$) the real and imaginary parts of σ are equal and the natural logarithm of the amplitude and the phase show the same slope, any of them giving the correct diffusivity of the material.

III. EXPERIMENTAL RESULTS AND DISCUSSION

We have used the slope method presented in Sec. II to measure the in-plane/longitudinal thermal diffusivity of thin sheets/filaments using a lock-in thermography setup, whose scheme is depicted in Fig. 3. Materials exhibiting very different diffusivity values, from polymers to metals, including anisotropic samples, have been studied. An acousto-optically modulated laser beam (COHERENT, model Verdi, $\lambda=532$ nm) focused onto the sample surface by a spherical lens of 5 cm focal length has been used to heat the sample. The infrared emission from the sample surface is captured by an infrared camera (CEDIP, model JADE J550M, 3.6–5.0 μm) provided with a lens of 50 mm focal length. This lens has a minimum working distance of 23.5 cm, which gives a spatial resolution of 137 μm, i.e., each pixel measures the average temperature over a square on the sample of 137 μm in side. The lock-in software provided

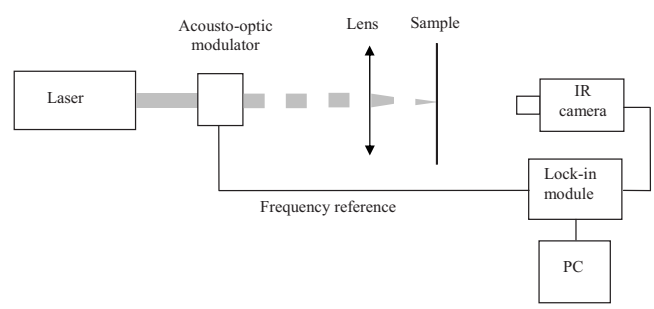

FIG. 3. Block diagram of the experimental setup.

Author complimentary copy. Redistribution subject to AIP license or copyright, see http://rsi.aip.org/rsi/copyright.jsp

with the camera gives the amplitude and phase of the oscillating temperature. To improve the signal to noise ratio we record 4000 images for each experiment. As the noise level is inversely proportional to the square root of the total number of images[16] we obtain a temperature noise level as low as 1 mK.

In the case of slabs, the measurements were carried out by heating the front face of the sample and recording the infrared emission from the rear surface. In the case of filaments, the laser is focused on one side of the sample and the infrared radiation is collected in the direction perpendicular to the laser beam, in order to prevent the laser beam to reach the camera lens. On the other hand, to increase the absorption to the exciting light and the infrared emissivity, slabs were covered by a 200 nm thick graphite layer, either on both sides (metals and alloys) or only on the surface facing the camera (polymers). The filaments used in this work were not covered since the signal to noise ratio was high enough for all kind of samples.

A. Effect of the surrounding air

We have performed lateral scans of the surface temperature at different frequencies (in the range from 0.1 Hz to 1 kHz) of a whole set of foils and wires. According to the theoretical results presented in Sec. II, the thermal diffusivity should remain constant as a function of the modulation frequency except at high frequencies, where the effects of diffraction are significant. While this prediction was fulfilled by good thermal conductors, whose thermal diffusivity was obtained accurately, an anomalous behavior was found for poor conductors. As a representative example, in Fig. 4(a) we show the thermal diffusivity obtained from the slopes of the amplitude and phase of the surface temperature, as well as the diffusivity obtained from the product of both slopes as a function of the modulation frequency for a monofilament of 150 μm of diameter of polyeter-eter-ketone (PEEK), a well known polymer. As expected, the diffraction effects are significant at high frequencies leading to an overestimation of the diffusivity, as observed by other authors.[3–7] However, at frequencies below 10 Hz the thermal diffusivity is almost constant, but its value (about 0.80 mm^2/s) is significantly higher than the value found in the literature (0.19 mm^2/s).[17] Moreover, measurements performed in thinner PEEK samples (both fibers and films) show the same behavior as that shown in Fig. 4(a), but leading to an even higher overestimation of the thermal diffusivity, which reaches $D = 1.2$ mm^2/s for the fiber with a diameter of 34 μm. This overestimation of the diffusivity of polymers is similar as that found by other authors.[2,8] These results indicate that, in our experiment, the slopes of the amplitude and phase do not compensate for the surface heat losses, the situation becoming more dramatic for the higher surface to volume ratio samples, where heat losses are more important.

In order to discriminate the source of this discrepancy we placed the sample in a vacuum chamber provided with sapphire windows, which are transparent to the infrared radiation. In Fig. 5 we show the amplitude and phase of the surface temperature of a 34 μm PEEK fiber at a modulation frequency of 0.12 Hz. Measurements were performed at room pressure (solid symbols) and at 3×10^{-3} mbar (open symbols). Several aspects deserve comment on this figure. First, the temperature rise is higher in vacuum due to the reduction in convective heat losses. Second, the signal-to-noise ratio is highly increased in vacuum since natural convection is a rather alleatory process introducing noise in the data. Third, the distortion of the amplitude and phase straight

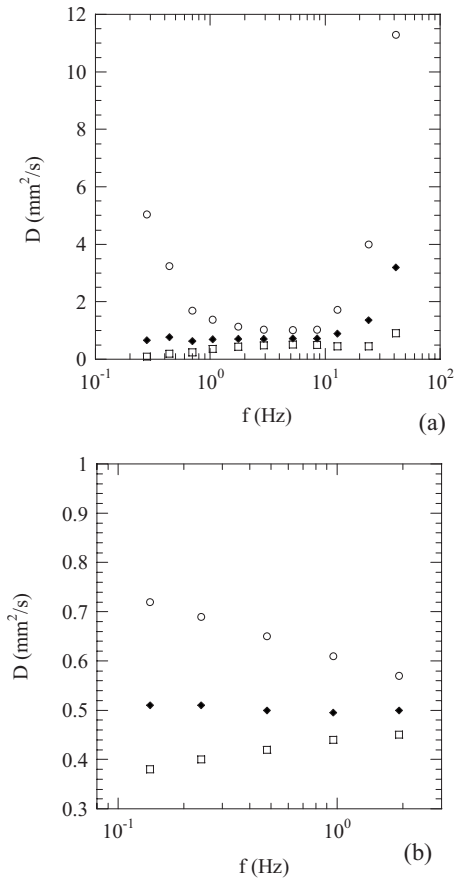

FIG. 4. Thermal diffusivity obtained from the slope of the surface temperature amplitude (squares), phase (circles), and from the product of the slopes (solid symbols), as a function of the modulation frequency. (a) 150 μm diameter PEEK filament in air, and (b) the same filament in vacuum (3×10^{-3} mbar).

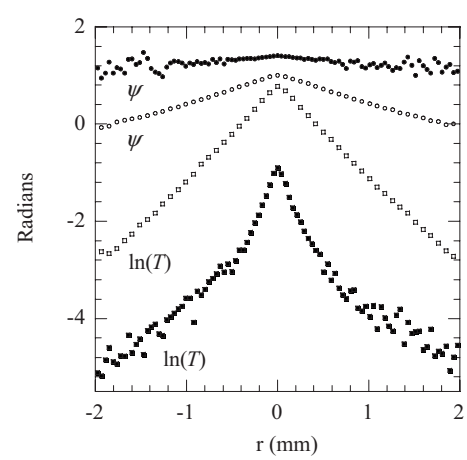

FIG. 5. Natural logarithm of the amplitude and phase of the surface temperature of a 34 μm diameter PEEK filament measured in vacuum (open symbols) and in air (solid symbols) at a modulation frequency of 0.12 Hz.

Author complimentary copy. Redistribution subject to AIP license or copyright, see http://rsi.aip.org/rsi/copyright.jsp

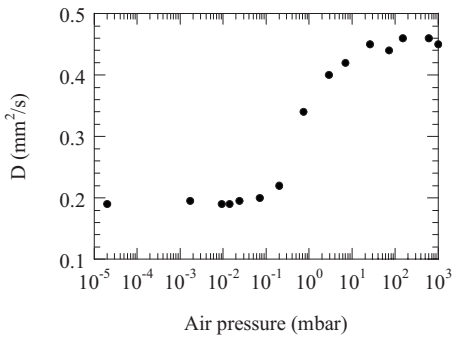

FIG. 6. Thermal diffusivity dependence on the air pressure for a 25 μm thick PEEK film.

lines profiles is absent in vacuum, allowing a more accurate determination of the thermal diffusivity from the slope method. Finally, the change in slope in vacuum of both, the amplitude and the phase of the surface temperature leads to a reduction of the thermal diffusivity overestimation (0.50 mm^2/s in vacuum instead of 1.2 mm^2/s in air). It is worth noting that although convection has been eliminated, the slopes of amplitude and phase remain very different, indicating that radiative heat losses are significant.

To better illustrate the effect of convection we have measured the thermal diffusivity of a 25 μm thick PEEK film as a function of the air pressure inside the vacuum chamber, from room pressure down to 10^{-5} mbar. Measurements have been performed at 0.12 Hz. The results are depicted in Fig. 6, showing a sigmoidal shape, meaning that the effect of the surrounding air saturates both at high and low pressures. Keeping the sample in vacuum i.e., removing the convective heat losses (pressure bellow 10^{-2} mbar), the correct thermal diffusivity of the PEEK film (0.19 mm^2/s) is obtained. In Fig. 4(b) we show the thermal diffusivity measurements of the same PEEK monofilament as in Fig. 4(a), but performed in vacuum. As expected, in both cases the difference in the diffusivities obtained from the amplitude slope and from the phase slope decrease as the modulation frequency increases but, more important, these differences are smaller in vacuum than in air, the only heat loss source in this case being the radiative one.

In Table I we show the measured values of the thermal diffusivity of several films and fibers of PEEK, in air and in vacuum (3×10^{-3} mbar). As can be seen the overestimation of the thermal diffusivity of the films is completely removed as convection losses are suppressed. These results confirm that convective heat losses are not properly described by the

TABLE I. Thermal diffusivity (mm^2/s) of several PEEK films and filaments measured in air and in vacuum. The literature value is 0.19 mm^2/s (Ref. 17). The uncertainty is 5%.

Shape	In air	In vacuum
Film $\ell=250$ μm	0.20	0.19
Film $\ell=125$ μm	0.26	0.19
Film $\ell=75$ μm	0.30	0.19
Film $\ell=25$ μm	0.45	0.19
Filament $2b=150$ μm	0.75	0.50
Filament $2b=34$ μm	1.2	0.50

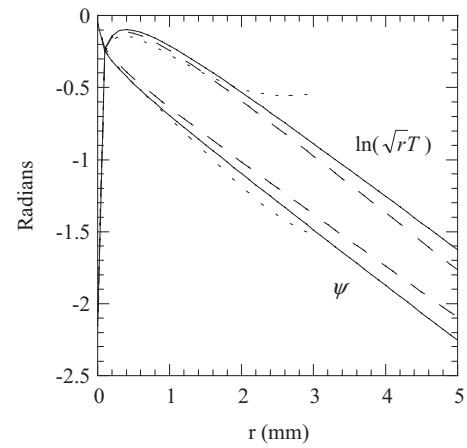

FIG. 7. Calculated amplitude (upper curves) and phase (lower curves) of the surface temperature of a 100 μm thick nickel foil at $f=1$ Hz, with $a=20$ μm. Three cases are considered: Infinite foil without heat losses (solid line), infinite foil with $h=2$ W/m^2 K (dashed line) and finite foil (16×7 mm^2) with $h=2$ W/m^2 K (dotted line).

linear term usually used to account for surface losses [hT in Eqs. (2) and (9)]. The high value of the thermal diffusivity of the PEEK filaments will be discussed later in this section.

B. Effect of the graphite layer

For all measurements performed with thin slabs a very thin graphite layer of about 200 nm was deposited by the sputtering method in order to improve both the absorption of the laser beam and the infrared emission. Its influence on the thermal diffusivity values obtained is negligible. However, care must be taken when using thicker black layers. Actually, covering the samples with a black paint layer is much quicker and cheaper than deposing graphite by the sputtering method, but the thickness of the paint layer is hardly thinner than 10 μm. In that case, its influence on the thermal diffusivity of films thinner than 100–150 μm is not negligible. By painting the PEEK films of thicknesses 125, 75, and 25 μm, with $a\sim10$ μm paint layer, we have obtained overestimated thermal diffusivity values of 0.21, 0.25, and 0.28 mm^2/s, respectively. For the 250 μm thick PEEK foil the accurate value was found instead. On the contrary, for metallic foils 100 μm thick, the contribution of the paint layer is almost insignificant since the effective diffusivity of the two layer system is dominated by the high diffusivity material. Only in the case of the thinnest metallic sample (10 μm thick Ni foil) a significant underestimations of the diffusivity was found.

C. Long distance approximation

The use of the slope method requires guaranteeing that the amplitude and phase behave linearly as a function of r, i.e., experimental data are taken far away from the excitation spot. As an example, we show in Fig. 7 the calculated lateral scan of the phase and of $\ln(\sqrt{rT})$ for a nickel foil 100 μm thick. Calculations have been performed by using Eq. (3) with $f=1$ Hz and $a=20$ μm. Simulations for both, adiabatic boundary conditions ($h=0$, solid line) and radiative heat losses ($h=2$ W/m^2 K, dashed line) are performed. As can be

Author complimentary copy. Redistribution subject to AIP license or copyright, see http://rsi.aip.org/rsi/copyright.jsp

seen the linear behavior only appears at distances from the heating spot verifying $r > \mu$. If experimental points closer to the heating spot were used in the linear regression, an inaccurate thermal diffusivity value would be obtained.

D. Boundary effects

More disturbing can be the effect of the sample boundaries. The slope method requires the use of low frequencies to avoid the diffraction effects, especially for poor thermal conductors. Under these conditions, the thermal wave propagates a long distance from the exciting region before vanishing, in such a way that it can reach the lateral boundaries of the sample. The dotted lines in Fig. 7 show the calculations of the amplitude and phase of the surface temperature for the same nickel foil, with radiative heat losses ($h=2$ W/m^2 K), but with a finite lateral size of 16×7 mm^2. The amplitude and phase profiles correspond to the shortest dimension of the sample. The effect of the sample boundaries has been accounted for by using the image method,[18] which requires adiabatic boundary conditions at the sample side surfaces. This assumption is plausible since the sample sides have a very small area (sample thickness is 100 μm) for the heat to be efficiently transferred from the sample contour. As can be seen, the slope of the phase decreases and that of $\ln(\sqrt{r}T)$ increases if compared to the infinite sample without heat losses, i.e., their behavior is reversed, with respect to an infinite sample affected by heat losses. In consequence, at low modulation frequencies, the thermal diffusivity obtained from the slope of the phase is lower than the one obtained from the slope of the amplitude. Moreover, the "inversion" of the amplitude and phase slopes is also accompanied with a loss of linearity of both the phase and $\ln(\sqrt{r}T)$ as a function of r. The frequency at which this inversion takes place increases as the thermal diffusivity becomes higher and the dimensions decrease. If the modulation frequency is increased in the calculations, all slopes approach to each other, as the effects of both, sample dimensions and heat losses become less significant.

Figure 8 shows the measured thermal diffusivity of a 16 mm$\times$7 mm$\times$100 μm nickel foil, obtained from the slopes of the amplitude, of the phase and from the product of both. At frequencies higher than 100 Hz diffraction effects are present. At intermediate frequencies the correct thermal diffusivity (22 mm^2/s) is obtained. However, at frequencies below 3 Hz (corresponding to a thermal diffusion length of $\sim$1.5 mm), the behavior of the slopes of the amplitude and phase is reversed and higher diffusivities are obtained from the slopes of the amplitudes. Moreover, the diffusivity obtained from the product of both slopes increases as the modulation frequency decreases. This result is explained by the combination of the two last effects: the long distance approximation is not longer valid and the side effects are not negligible.

E. Anisotropic thin plates

According to the theoretical results obtained in Sec. II B, the slope method can also be used to measure the thermal diffusivity of anisotropic thin plates along the principal axes

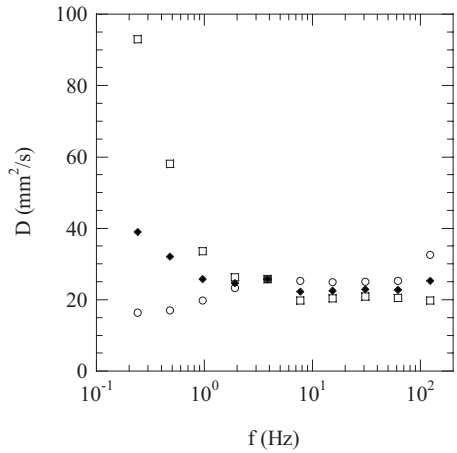

FIG. 8. Experimental values of the thermal diffusivity of a 16 mm $\times$7 mm$\times$100 μm nickel foil as a function of the modulation frequency obtained from the slopes of the $\ln(\sqrt{r}T)$ (open squares), from the slope of the phase (open circles) and from the product (solid symbols), along the shortest sample dimension.

contained in the surface. In this way, we have characterized the thermal diffusivity tensor of two well known orthotropic materials: a 100 μm thick slab of pyrolytic graphite (PG), a 30 μm thick slab of pyrolytic boron nitride (PBN), and of a 175 μm thick carbon fiber reinforced polymer composite. As an example, in Fig. 9 we show the surface phase thermogram corresponding to the PEEK composite sample, at a modulation frequency of 13 Hz, where elliptical isophases, characteristic of anisotropic materials can be clearly observed. Due to the very high thermal anisotropy ratio of these samples, different modulation frequencies must be used to measure the two principal thermal diffusivities accurately. For the fiber reinforced composite, the lower (higher) thermal diffusivity was measured at modulation frequencies below (above) 1 Hz. The corresponding thermal diffusivity values obtained along the two principal directions were 5.5 and 0.55 mm^2/s, which are in good agreement with the values of the diffusivity obtained for this sample using the mirage technique.[19] Similarly, for PG and PBN, frequencies ranging from 5 to 100 Hz are better suited for the highest thermal diffusivity measurements (203 mm^2/s for PG and 65 mm^2/s for PBN). Actually using lower frequencies leads to boundary effects. On the contrary, for the lowest thermal diffusivity (1.6 mm^2/s for PG and 1.2 mm^2/s for PBN) frequencies below 3 Hz are used to avoid diffraction effects.

F. Final remarks

Limiting the temperature rise of the sample surface during the experiments guarantees that nonlinear effects associ-

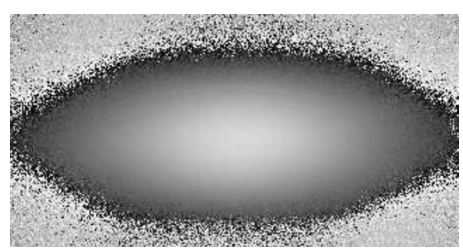

FIG. 9. Experimental surface phase thermogram for the carbon fiber reinforced PEEK slab, 175 μm thick, at a modulation frequency of 13 Hz.

Author complimentary copy. Redistribution subject to AIP license or copyright, see http://rsi.aip.org/rsi/copyright.jsp

TABLE II. Thermal diffusivity (mm^2/s) of several thin slabs and filaments. Measurements performed in vacuum. Slabs have been covered by a 200 nm thick graphite layer. The error is 5%.

Material	Shape	This work	Literature[a]
Cu	Foil $\ell=100$ μm	122	116
Ni	Foil $\ell=100$ μm	22	22
Ni	Foil $\ell=10$ μm	21	22
AISI-302	Foil $\ell=100$ μm	3.8	3.7–4.0
PEEK	Film $\ell=250$ μm	0.19	0.19
PEEK	Film $\ell=125$ μm	0.19	0.19
PEEK	Film $\ell=75$ μm	0.19	0.19
PEEK	Film $\ell=25$ μm	0.19	0.19
Pyrolytic graphite	Film $\ell=100$ μm	203	215
		1.6	1.5
Pyrolytic boron	Film $\ell=30$ μm	65	–
Nitride		1.2	–
PEEK composite	Film $\ell=175$ μm	5.5	6
		0.55	0.4
Ni	Wire $2b=125$ μm	19	22
Ti	Wire $2b=125$ μm	8.8	9.0
AISI-302	Wire $2b=125$ μm	3.75	3.7–4.0
	Wire $2b=25$ μm	3.5	3.7–4.0
PEEK	Filament $2b=150$ μm	0.50	0.19
PEEK	Filament $2b=34$ μm	0.50	0.19
Human hair	Filament $2b=60$ μm	0.14	–

[a]References 15, 17, 18, 25, and 26.

ated to the dependence of the thermal properties on temperature are negligible. In our setup, we limit the maximum temperature rise above the ambient (that is produced at the heating laser spot) to a value of about 2 K. This means that the laser power is varied according to the properties of the sample (thermal diffusivity, shape, thickness, and diameter) and to the modulation frequency used. Laser power values between a few milliwatts for thin polymers and 350 mW for the thicker metals have been used.

In Table II we summarize the thermal diffusivity values obtained with our lock-in thermography setup under the best experimental conditions: vacuum chamber, 200 nm graphite layer covering the foils, minimum laser power, big enough samples to avoid boundary effects, etc. As can be seen, the agreement with literature values is very good for both good and poor thermal conductors. The only discrepancy appears for the PEEK filaments, for which a thermal diffusivity 2.5 higher than the nominal one has been obtained. It is worth noting that the value is independent of the diameter, indicating it is not related to heat losses. It has been demonstrated that crystalline polymers increase their thermal diffusivity after drawing process.[20,21] As our PEEK filaments, whose degree of crystallinity has been measured to be 45%, are obtained by extrusion, we attribute the high value of the measured diffusivity to the structural changes induced during the fabrication process of the filaments.

It is worth mentioning the result obtained for the human hair. Although no reliable thermal diffusivity is available in the literature, the very low value we have obtained is consistent with the combination of the low thermal diffusivity of the keratin (the material the hair is made of) and the complicated internal structure of hair, with many layers introducing thermal resistances, which reduce the thermal diffusivity.[22]

Finally, we would like to mention that, for all slabs listed in Table II, we have also performed thermal diffusivity measurements by focusing the laser beam with a cylindrical lens on the sample surface, in such a way that an almost uniform line beam was illuminating the whole sample width, leading to a 1D heat propagation. The values of the diffusivity we obtained were very similar to the ones obtained in the case of 2D propagation.

The conclusions of this paper are also valid for every technique measuring the surface temperature. For instance, a thermocouple attached at the rear surface has been used to measure the thermal diffusivity.[18,23,24] However, noncontact techniques such as infrared thermography are preferable when dealing with thin samples.

IV. SUMMARY AND CONCLUSIONS

We have analyzed the effects of the experimental conditions on the thermal diffusivity measurements of thin slabs and filaments using the slope method in lock-in thermography experiments. As a result, we have demonstrated that convective heat losses are not properly described by the linear heat loss term introduced in the model, which has been extended to the case of 2D propagation. We have shown that, when using the slope method, the effect of convective heat losses is to increase the apparent diffusivity of the samples, thus elucidating the origin of literature overestimation of the diffusivity of bad thermal conductors. We have concluded that reliable values of the thermal diffusivity of isotropic and anisotropic thin slabs and filaments of any thermal properties can be found provided several experimental conditions, imposed by the theoretical model, are fulfilled: (a) the sample is kept in vacuum to suppress convective heat losses, especially low diffusivity materials, (b) the thickness of the black layer deposited to increase the infrared emission must be negligible with respect to the sample thickness, (c) only experimental data far away from the heating spot, where amplitude and phase behave linearly, are used, (d) small laser powers, producing small temperature rise, are used to prevent nonlinear heating effects, (e) high modulation frequencies ($f > 10$ Hz) are avoided, especially for poor conductor materials, to avoid diffraction effects, and (f) low frequencies (0.1–1 Hz) are preferred provided the slabs are large enough to avoid boundary effects. Lock-in thermography measurements performed on a wide set of thin slabs and filaments of different thicknesses and thermal properties in the suitable experimental conditions, confirm the validity of the slope method to perform accurate evaluation of the thermal diffusivity from lock-in thermography data.

ACKNOWLEDGMENTS

This work has been supported by the Ministerio de Educación y Ciencia (Grant No. MAT2008-01454) and by the Universidad del País Vasco (Grant No. DIPE08/10).

[1] L. Fabbri and P. Fenici, Rev. Sci. Instrum. **66**, 3593 (1995).
[2] B. Zhang and R. E. Imhof, Appl. Phys. A: Mater. Sci. Process. **62**, 323 (1996).
[3] J. F. Bisson and D. Fournier, J. Appl. Phys. **83**, 1036 (1998).

Author complimentary copy. Redistribution subject to AIP license or copyright, see http://rsi.aip.org/rsi/copyright.jsp

[4] J. F. Bisson and D. Fournier, J. Appl. Phys. **84**, 38 (1998).
[5] H. G. Walther and T. Kitzing, J. Appl. Phys. **84**, 1163 (1998).
[6] S. Paoloni and D. Fournier, J. Appl. Phys. **92**, 5950 (2002).
[7] S. Paoloni and D. Fournier, J. Appl. Phys. **92**, 5955 (2002).
[8] A. Wolf, P. Pohl, and R. Brendel, J. Appl. Phys. **96**, 6306 (2004).
[9] A. Muscio, P. G. Bison, S. Marinetti, and E. Grinzato, Int. J. Therm. Sci. **43**, 453 (2004).
[10] C. Pradère, J. M. Goyhénèche, J. C. Batsale, S. Dilhaire, and R. Pailler, Int. J. Therm. Sci. **45**, 443 (2006).
[11] M. Oksanen, R. Scholz, and L. Fabbri, J. Mater. Sci. Lett. **16**, 1092 (1997).
[12] J. Hou, X. Wang, and J. Guo, J. Phys. D **39**, 3362 (2006).
[13] W. B. Jackson, N. M. Amer, A. C. Boccara, and D. Fournier, Appl. Opt. **20**, 1333 (1981).
[14] *Handbook of Mathematical Functions*, edited by M. Abramowitz and I. A. Stegun (Dover, New York, 1965), p. 378.
[15] A. Salazar, A. Sánchez-Lavega, A. Ocáriz, J. Guitonny, G. C. Pandey, D. Fournier, and A. C. Boccara, J. Appl. Phys. **79**, 3984 (1996).
[16] O. Breitenstein and M. Langenkamp, *Lock-in thermography* (Springer, Berlin, 2003), p. 32.
[17] See: *Technical data: material properties of PEEK*, Goodfellow Corporation, URL: http://www.goodfellow.com.
[18] H. Kato, T. Baba, and M. Okaji, Meas. Sci. Technol. **12**, 2074 (2001).
[19] A. Salazar and A. Sánchez-Lavega, Int. J. Thermophys. **19**, 625 (1998).
[20] C. L. Choy, G. W. Yang, and Y. W. Wong, J. Polym. Sci., Part B: Polym. Phys. **35**, 1621 (1997).
[21] C. L. Choy, Y. W. Wong, G. W. Yang, and T. Kanamoto, J. Polym. Sci., Part B: Polym. Phys. **37**, 3359 (1999).
[22] S. Nagase, M. Oshika, S. Ueda, N. Satoh, and K. Tsujii, Bull. Chem. Soc. Jpn. **73**, 2161 (2000).
[23] I. Hatta, Y. Sasuga, R. Kato, and A. Maesono, Rev. Sci. Instrum. **56**, 1643 (1985).
[24] Y. Gu and I. Hatta, Jpn. J. Appl. Phys., Part 1 **30**, 1295 (1991).
[25] L. R. Touloukian, R. W. Powell, C. Y. Ho, and M. C. Nicolasu, *Thermal Diffusivity* (IFI/Plenum, New York, Washington, 1973).
[26] A. Salazar, A. Sánchez-Lavega, A. Ocáriz, J. Guitonny, J. C. Pandey, D. Fournier, and A. C. Boccara, Appl. Phys. Lett. **67**, 626 (1995).

Author complimentary copy. Redistribution subject to AIP license or copyright, see http://rsi.aip.org/rsi/copyright.jsp